

# Depth Priors in Removal Neural Radiance Fields

Zhihao Guo<sup>1</sup> and Peng Wang<sup>2</sup>

Department of Computing and Mathematics, Manchester Metropolitan University,  
zhihao.guo@stu.mmu.ac.uk

**Abstract.** Neural Radiance Fields (NeRF) have shown impressive results in 3D reconstruction and generating novel views. A key challenge within NeRF is the editing of reconstructed scenes, such as object removal, which requires maintaining consistency across multiple views and ensuring high-quality synthesised perspectives. Previous studies have incorporated depth priors, typically from LiDAR or sparse depth measurements provided by COLMAP to improve the performance of object removal in NeRF. However, these methods are either costly or time-consuming. In this paper, we propose a novel approach that integrates monocular depth estimates with NeRF-based object removal models to significantly reduce time consumption and enhance the robustness and quality of scene generation and object removal. We conducted a thorough evaluation of COLMAP’s dense depth reconstruction on the KITTI dataset to verify its accuracy in depth map generation. Our findings suggest that COLMAP can serve as an effective alternative to a ground truth depth map where such information is missing or costly to obtain. Additionally, we integrated various monocular depth estimation methods into the removal NeRF model, i.e., SpinNeRF to assess their capacity to improve object removal performance. Our experimental results highlight the potential of monocular depth estimation to substantially improve NeRF applications.

**Keywords:** Neural Radiance Fields · Monocular Depth Estimation · 3D Editing · 3D Reconstruction

## 1 Introduction

Neural Radiance Fields (NeRF) [1] has been transformative for 3D reconstruction and novel view synthesis, especially in robot environment perception and the construction of stable robot digital twin systems that are critical for the next generation of robotic autonomy [2]. However, how to seamlessly remove objects in rendered NeRF is still a substantial challenge which could be desirable for several reasons. For instance, planning a safe path for robots in a human-robot collaborative shared environment necessitates the removal of specific obstacles.

Recent works have addressed this issue [3,4,5], with most methods employing depth priors to supervise the rendered quality of geometry. Typically, depth is provided by raw LiDAR or depth completion techniques trained with sparse COLMAP depth [6]. Furthermore, current methods frequently encounter difficulties in securing readily accessible depth maps, essential for preserving the

integrity of altered scenes, especially regarding lighting and shadow consistency, which are critical elements for realistic rendering and precise perception. Consequently, a thorough evaluation of the effect of various depth priors on Removal NeRF is imperative.

In this paper, we utilize the architecture of SpinNeRF as the foundational removal NeRF model. Depth priors derived from various models, such as ZoeDepth, are first integrated into SpinNeRF to enhance its performance in object removal tasks, evaluated across a range of metrics. A comprehensive evaluation of COLMAP’s dense depth reconstruction on the KITTI dataset [7] assesses its precision and detail in generating depth maps. Our findings reveal that COLMAP achieves superior performance, establishing it as a feasible alternative to traditional ground truth depth acquisition, especially in contexts where obtaining such depth maps is cost-prohibitive. Additionally, we explore various monocular depth estimation methods on the SpinNeRF dataset [4] to identify the most effective technique for supplying depth priors. ZoeDepth is identified as the state-of-the-art monocular depth estimation method, offering high-quality depth priors to SpinNeRF while also minimizing computational demands. Crucially, our integration of ZoeDepth with SpinNeRF significantly enhances the robustness and quality of rendered NeRF scenes and object removal. These findings highlight the potential of monocular depth estimation to significantly augment NeRF applications.

The **contributions** of this work include 1). The architecture of SpinNeRF is utilized, and depth priors from ZoeDepth are integrated to enhance object removal capabilities within SpinNeRF while also reducing computational overhead; 2). A detailed evaluation of COLMAP’s dense depth reconstruction on KITTI dataset demonstrates that COLMAP serves as a cost-effective alternative to traditional Ground Truth depth acquisition, particularly in contexts where acquiring such data proves economically prohibitive; 3). Exploring various monocular depth estimation methods on SpinNeRF dataset to ascertain the most efficacious approach for supplying depth priors. ZoeDepth emerges as the preeminent method, distinguished by its generation of high-quality depth priors.

The remainder of the paper is organised as follows. Some related works are introduced in Section 2. Section 3 elaborates on the impacts of depth priors on the removal performance of NeRF, and the methodology integrating SpinNeRF with ZoeDepth is presented. Experiments, discussions, and an ablation study are provided in Section 4, and the paper is concluded in Section 5.

## 2 Related Works

### 2.1 Neural Radiance Fields

**Depth Supervised NeRF** NeRF [1] utilise implicit representation for the first time to achieve photo-realistic perspective synthesis. Given 3D location  $\mathbf{p} = (x, y, z)$  and 2D view direction  $\mathbf{d} = (\theta, \phi)$ , NeRF predicts the color  $\mathbf{c} = (r, g, b)$  of a sampling point and the volume density  $\sigma$  through a multi-layer perceptron [8]

which can be represented as

$$F_{\Theta} : (\mathbf{p}, \mathbf{d}) \rightarrow (\mathbf{c}, \sigma) \quad (1)$$

To optimize its weights  $\Theta$  to map from each input 5D coordinate to its corresponding density and color, the expected color is estimated by volumetric rendering via quadrature, the color rendering is formulated as:

$$C(\mathbf{r}) = \int_{t_n}^{t_f} T(t) \sigma(\mathbf{r}(t)) \mathbf{c}(\mathbf{r}(t), \mathbf{d}) dt, \quad (2)$$

where  $T(t) = \exp\left(-\int_{t_n}^t \sigma(\mathbf{r}(s)) ds\right)$ ,  $C(\mathbf{r})$  is the sampling pixel value and is calculated by integrating the radiance value  $\mathbf{c}$  along the ray  $\mathbf{r}(t) = \mathbf{o} + t\mathbf{d}$ ,  $\mathbf{o}$  is the camera position,  $\mathbf{d}$  is the direction of the sampled pixel, within near and far bounds  $t_n$  and  $t_f$ , and the function  $T(t)$  denotes the accumulated transmittance along each ray from  $t_n$  to  $t$ . However, training NeRF could be difficult when given insufficient input images, DSNeRF [6] first utilise additional supervision depth priors recovered from 3D point clouds, estimated from SfM to render better images.

**Removal NeRF** Removal NeRF is a variant of NeRF, and it aims at editing objects synthesised by NeRF models. There are a range of removal NeRF models and they can be briefly classified into two categories: 1) Learn an object compositional NeRF, such as Object-NeRF [3] and ObjectSDF [9], these works produce realistic rendering with editing capability for a clustered and real world scene, however, can not render view-consistent images; 2) Utilise the inpainted images and depth priors, such as SPinNeRF [4] and NeRF-Object-Removal [5] utilise 2D inpainting method LAMA [10] to generate the inpainted depth priors and render better quality removal NeRF results.

## 2.2 Depth Estimation

**COLMAP Dense Depth** COLMAP is an end-to-end multi-view image-based 3D reconstruction technique that is built on top of Structure-from-Motion (SfM) [11] and Multi-View Stereo (MVS) reconstruction [12]. In addition, it can also achieve depth estimation, which is required by 3D synthesis models such as NeRF. We will briefly go through the pipeline of COLMAP as it is used for depth acquisition in this paper.

SfM mainly entails the following procedures: feature extraction  $F_i$ , feature matching  $M_{ij}$ , robust model estimation, and bundle adjustment. Feature extraction, denoted as  $F_i$ , aims at extracting features such as SIFT from a given image  $I_i$ . The features from image  $I_i$  will be next matched with features from another image(s)  $I_j$ , and we denote the matching process as  $M_{ij}$ . The matched features will be used to create a sparse 3D point cloud using triangulation[13], which is denoted as

$$P_{ij} = T(M_{ij}, C_i, C_j), \quad (3)$$

where  $P_{ij}$  are the 3D points triangulated from matches  $M_{ij}$ , and  $C_i, C_j$  are the camera parameters associated with images  $I_i$  and  $I_j$ , respectively. The bundle adjustment procedure refines camera parameters and 3D points simultaneously to minimise the re-projection error, and each minimization term individually considers camera parameter  $c_i$  to simplify the optimization problem and expedites the computational process, which is denoted as

$$\min_{C_i, P_{ij}} \sum_{i,j} d(Q(M_{ij}, C_i), P_{ij}), \quad (4)$$

where  $d(\cdot)$  is the Euclidean distance, and  $Q(\cdot, \cdot)$  is the projection function that projects 3D points  $P_{ij}$  onto the image plane using camera parameter  $C_i$ .

**Monocular Depth Estimation** Depth estimation from monocular images has led to a variety of approaches. Early monocular depth estimation works [14,15] relied on handcrafted features, which lack generality to unpredictable and variable conditions in natural scenes. The limitations of these methods have prompted the exploration of deep learning methods [16,17,18,19,20] in depth estimation.

Some recent works focus on encoder-decoder models [17,18], for instance, ZoeDepth [18] introduces a novel architecture combines relative and metric depth, following MiDaS depth estimation framework [21] to predict relative depth, and add heads to the encoder-decoder model for metric depth estimation, which is achieved by attaching a metric bins module to the decoder. The final depth of a pixel  $i$  is obtained by a linear combination of the bin centers weighted by the corresponding predicted probabilities,

$$d(i) = \sum_{k=1}^{N_{\text{total}}} p_i(k) c_i(k), \quad (5)$$

where  $d(i)$  is the predicted depth at pixel  $i$ ,  $N_{\text{total}}$  is the total number of depth bins,  $p_i(k)$  is the probability of the  $k$ -th bin for pixel  $i$ , and  $c_i(k)$  is the center of the  $k$ -th depth bin. DepthAnything [17] is another deep learning-based model depth estimation model. It learns from both unlabeled image datasets  $\mathcal{D}^u = \{u_i\}_{i=1}^N$  and labeled datasets  $\mathcal{D}^l = \{(x_i, d_i)\}_{i=1}^M$ . A teacher model  $T$  is first learned from  $\mathcal{D}^l$ , which is next used to assign pseudo depth labels for  $\mathcal{D}^u$ . The depth estimation model will then be trained on the combination of labeled datasets and pseudo-unlabeled datasets. Recently, EcoDepth [16] presents a new architecture module called Comprehensive Image Detail Embedding (CIDE) and formulates monocular depth estimation as a dense regression problem,

$$\mathbb{P}(\mathbf{y} \mid \mathbf{x}, \mathcal{E}) = \mathbb{P}(\mathbf{y} \mid \mathbf{z}_0) \mathbb{P}(\mathbf{z}_0 \mid \mathbf{z}_t, \mathcal{C}) \mathbb{P}(\mathbf{z}_t \mid \mathbf{x}) \mathbb{P}(\mathcal{C} \mid \mathbf{x}), \quad (6)$$

where  $\mathbf{x}$  and  $\mathbf{y}$  denote input image and output depth,  $\mathcal{C}$  represents the semantic embedding derived from CIDE module,  $\mathbb{P}(\mathbf{y} \mid \mathbf{z}_0)$  is implemented through the Depth Regressor module, which is a two-layer convolutional neural network (CNN),  $\mathbb{P}(\mathcal{C} \mid \mathbf{x}) = \mathbb{P}(\mathcal{C} \mid \mathcal{E}) \mathbb{P}(\mathcal{E} \mid \mathbf{x})$ ,  $\mathbb{P}(\mathbf{z}_t \mid \mathbf{x})$  is implemented using VAE's



encoder [22],  $\mathcal{C}$  is the conditional information generated by CIDE, and  $\mathcal{E}$  is the embedding vector of a ViT module [23],  $\mathbb{P}(\mathcal{C} \mid \mathcal{E})$  is implemented using downstream modules in CIDE consisting of learnable embeddings,  $\mathbb{P}(\mathbf{z}_0 \mid \mathbf{z}_t, \mathcal{C})$  is implemented using conditional diffusion, the final depth map  $y$  is obtained through an Upsampling Decoder, this decoder includes deconvolution layers and performs a resolution transition, specifically transitioning from a lower resolution of the concatenated feature map back to the original dimensions of the input image.

### 3 Removal NeRF with Monocular Depth Priors

This paper investigates how depth priors affect the object removal performance of NeRF models. To this end, the architecture of SpinNeRF [4] is employed as the base NeRF model. Depth priors obtained by different models such as ZoeDepth are next introduced to SpinNeRF, and the new model’s performance on object removal is then evaluated against a series of metrics.

SpinNeRF is a cutting-edge NeRF model designed to enhance the rendering of 3D scenes from sparse viewpoints. Unlike traditional NeRF models, SpinNeRF introduces a unique capability to interpolate and extrapolate views dynamically by learning the underlying structure of a scene through sparse image inputs. To be specific, given a set of RGB images  $\mathcal{I} = \{I_i\}_{i=1}^n$ , with the corresponding camera poses  $\mathcal{G} = \{G_i\}_{i=1}^n$  and camera intrinsic matrix  $K$  estimated by SfM, and the corresponding removal object mask  $\mathcal{M} = \{M_i\}_{i=1}^n$  provided by users or learned by a different model, SpinNeRF leverages a deep learning framework to encode the volumetric properties of a scene into a neural network, allowing for highly realistic and computationally efficient 3D rendering. During the rendering process, SpinNeRF utilises LAMA[10] to achieve image inpainting, and the inpainted images are denoted as  $\{\tilde{I}_i\}_{i=1}^n$ , with  $\tilde{I}_i = \text{INP}(\mathcal{I}, \mathcal{M})$  denoting the inpainting process.

To improve the overall removal and rendering performance, SpinNeRF uses the perceptual loss, LPIPS [24] to optimise the masked regions during rendering, while MSE is still used for unmasked regions,

$$\mathcal{L}_{\text{LPIPS}} = \frac{1}{|\mathcal{B}|} \sum_{i \in \mathcal{B}} \text{LPIPS}(\hat{I}_i, \tilde{I}_i), \quad (7)$$

where  $\mathcal{B}$  is a subset of the entire dataset which are between 1 and  $n$ ,  $\hat{I}_i$  is the  $i$ -th view rendered using NeRF,  $\tilde{I}_i$  is the  $i$ -th view that has been inpainted.

To achieve high-quality image inpainting, depth information on objects of interest is required. In the SpinNeRF framework, the depth priors  $\{D_i\}_{i=1}^n$  are calculated using

$$D(r) = \sum_{i=1}^N T_i \left(1 - \exp(-\sigma_i \delta_i)\right) t_i. \quad (8)$$

The priors are then passed to INP to generate inpainted depth maps  $\{\tilde{D}_i\}_{i=1}^n$ , where  $\tilde{D}_i = \text{INP}(D_i, \mathcal{M})$ . The depth maps will be used to supervise the in-

---

**Algorithm 1** NeRF-based Object Removal using Monocular Depth Priors

---

- 1: **Inputs:** RGB training images  $\mathcal{I} = \{I_i\}_{i=1}^n$ , 3D poses  $\mathcal{G} = \{G_i\}_{i=1}^n$ , camera intrinsic matrix  $K$  and removal object mask  $\mathcal{M} = \{M_i\}_{i=1}^n$
  - 2: **for** each image in the training set **do**
  - 3:   Mask guided multi-view segmentation
  - 4:   Render the masks into the scene using a Semantic NeRF model LaTeRF [25] create a 3D-consistent mask
  - 5: **end for**
  - 6: Disparity rendering using ZoeDepth
  - 7: Using LaMa to generate inpainted RGB images and inpainted disparities
  - 8: Optimise the final inpainted NeRF
  - 9: **Outputs:** Inpainted images with objects removal
- 

inpainted NeRF, and the inpainting process is optimised using the  $\ell_2$  distance between the rendered depths  $D_i$  and the inpainted depths  $\tilde{D}_i$

$$\mathcal{L}_{\text{depth}} = \frac{1}{|\mathcal{R}|} \sum_{r \in \mathcal{R}} |D(r) - \tilde{D}(r)|^2, \quad (9)$$

where  $D(r)$  and  $\hat{D}(r)$  are the depth values for a ray  $r$ . The whole process is aggregated into Algorithm 1.

## 4 Experiments and Analysis

### 4.1 Dataset

We have conducted a comprehensive evaluation of the dense depth maps reconstructed utilising COLMAP on a subset of KITTI dataset, which comes with Ground Truth depth that can help to ascertain the accuracy and applicability of using depth obtained by COLMAP in real-world scenarios, especially in 3D view synthesis using depth as priors. The selected sequences comprised 1,048 frames, carefully chosen to represent diverse conditions and environments.

Through evaluations on the KITTI dataset, our assumptions are the dense depth maps generated by COLMAP are accurate enough to be considered as ground truth of depth for applications such as 3D view synthesis. To this end, we have used the second dataset used by SpinNeRF [4], which includes 10 different scenes with camera parameters and sparse reconstructed points from SfM. The ground truth depth maps of the dataset are generated by COLMAP dense reconstruction.

Based on the positive conclusion that dense depth generated by COLMAP can be considered as ground truth, we then evaluate how depth priors provided by other means such as monocular depth estimation methods affect object removal using NeRF models. A range of experiments have been conducted to support our assumptions above.

## 4.2 Evaluation Metrics

**Depth Metric** The disparities between depth generated by COLMAP (or real depth from KITTI when available) and monocular depth estimation models are evaluated using different metrics such as Root Mean Squared Error (RMSE), logarithmic scale error [26]. Additionally, the commonly adopted threshold-based accuracy metric  $\delta_1$  is further used. This metric specifically measure the proportion of predicted depth values that fall within predefined error thresholds relative to the ground truth. The metrics mentioned above are defined as follows

$$\text{RMSE} = \sqrt{1/N \sum_{i=1}^N (D_{\text{gt}_i} - D_{\text{pred}_i})^2}, \quad (10)$$

$$\delta_1 = \max(D_{\text{gt}_i}/D_{\text{pred}_i}, D_{\text{pred}_i}/D_{\text{gt}_i}) < 1.25, \quad (11)$$

$$\log_{10} \text{Error} = 1/N \sum_{i=1}^N |\log_{10}(D_{\text{gt}_i}) - \log_{10}(D_{\text{pred}_i})|, \quad (12)$$

where  $N$  is the number of images, and  $D_{\text{gt}_i}$  and  $\text{pred}_i$  are the  $i$ -th depth ground truth and predicted depth, respectively.

Considering the challenges in calculating the metrics introduced by very sparse ground truth depth values from KITTI, we have designed Algorithm 2 to calculate these values.

---

### Algorithm 2 Dense Depth Evaluation

---

- 1: **Inputs:** Predicted Depth Maps  $D_{\text{pred}_i}$ , Ground Truth Depth Maps  $D_{\text{gt}_i}$
  - 2: Initialize metrics lists for RMSE,  $\delta_1$ ,  $\delta_2$ ,  $\delta_3$ , and  $\log_{10}$
  - 3: **for** each frame in the dataset **do**
  - 4:   Load ground truth depth map  $D_{\text{gt}}$
  - 5:   Load predicted depth map  $D_{\text{pred}}$
  - 6:   Align dimensions of  $D_{\text{gt}}$  and  $D_{\text{pred}}$  by padding
  - 7:   Compute scaling factor  $s$  and adjust  $D_{\text{pred}}$  by  $s$
  - 8:   Crop to valid region in both  $D_{\text{gt}}$  and  $D_{\text{pred}}$
  - 9:   Compute performance metrics for the frame
  - 10: **end for**
  - 11: Calculate mean of metrics across all frames
  - 12: Print averaged metrics
- 

**NeRF Metric** The widely used metrics such as for synthesised image quality evaluation such as PSNR, SSIM [27] are used to evaluate the performance of object removal using NeRF with different depth priors. The definitions of PSNR and SSIM are as follows.

$$\text{PSNR} = 20 \cdot \log_{10} \left( \frac{\max_I}{\sqrt{\text{MSE}}} \right), \quad (13)$$

where  $\max_I$  is the maximum possible pixel value of the image, and MSE stands for the mean squared error between the original and reconstructed images.

$$\text{SSIM}(x, y) = \frac{(2\mu_x\mu_y + c_1)(2\sigma_{xy} + c_2)}{(\mu_x^2 + \mu_y^2 + c_1)(\sigma_x^2 + \sigma_y^2 + c_2)}, \quad (14)$$

where  $x$  is the original depth map pixel,  $y$  is the corresponding predicted depth map pixel.  $\mu_x$  is the average of  $x$ ,  $\mu_y$  is the average of  $y$ ,  $\sigma_x^2$  and  $\sigma_y^2$  are the variances of  $x$  and  $y$ ,  $\sigma_{xy}$  is the covariance of  $x$  and  $y$ ,  $c_1$  and  $c_2$  are variables to stabilize the division with a weak denominator.

### 4.3 Results and Discussions

**Depth Evaluation on KITTI Datasets** This set of experiments is meant to support our first assumption that the depth generated by COLMAP can be taken as depth ground truth in scenarios lacking ground truth information. This will further support our second assumption that we can take depth generated by COLMAP as ground truth to evaluate depth obtained by monocular depth estimation models.

We rigorously evaluate the depth maps obtained from COLMAP’s dense depth reconstruction and various monocular depth estimation methods, using the selected KITTI datasets with real ground truth depth maps. The evaluation results can be found in Table 1, which demonstrates that COLMAP’s dense depth reconstruction outperforms the monocular depth estimation methods across most evaluation metrics. To be specific, the  $\delta_1$  value for COLMAP is 91%, which is significantly higher than other methods, indicating that COLMAP’s depth maps are the closest to the Ground Truth. So in scenarios where ground truth depth acquisition is costly, **COLMAP’s dense depth reconstruction can effectively substitute for ground truth depth**. Further details and visual comparisons of depth maps obtained by different methods can be found in Figure 1. Take COLMAP dense depth map for an example, we can see in Figure 1, compared with other monocular depth estimation methods, the depth map obtained by COLMAP has a more accurate understanding and representation of the edges of objects in the image.

Table 1: Different Methods on Selected KITTI for Depth Estimation

Methods	RMSE ↓	$\delta_1$ ↑	$\log_{10}$ ↓
COLMAP	0.017	0.910	0.042
EcoDepth	0.017	0.670	0.080
ZoeDepth	0.024	0.807	0.064
Depth Anything	0.044	0.184	0.357

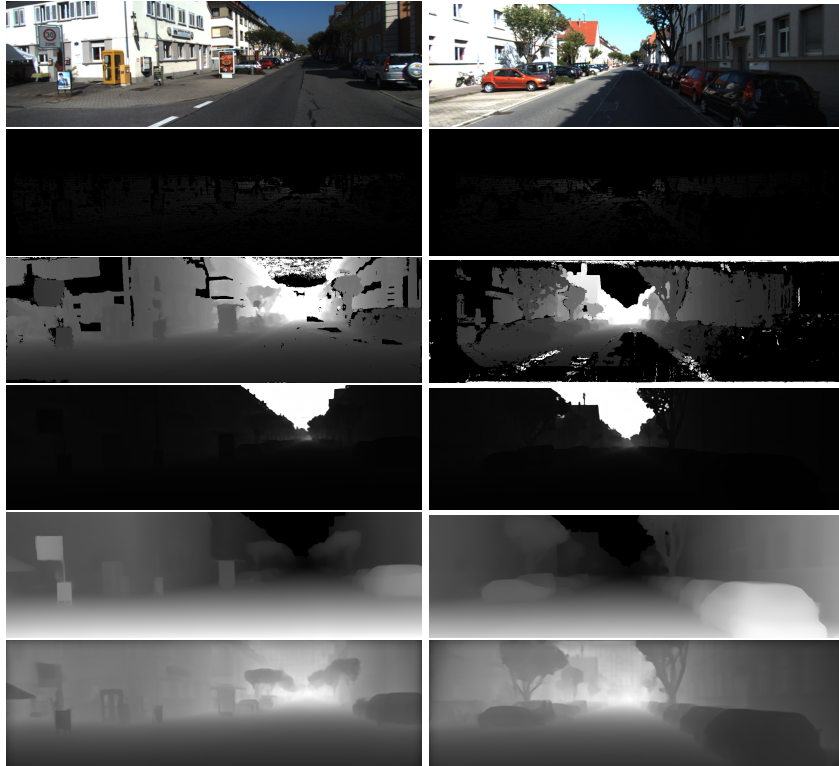


Fig. 1: Estimation Depth Map comparison on KITTI Selected Sequences. The first row is raw image, the second row is ground truth depth map, the third row is COLMAP dense depth map, the fourth row is EcoDepth depth map, the fifth row is DepthAnything depth map and the sixth row is ZoeDepth depth map.

**Depth Evaluation on Removal NeRF Dataset** We followed the findings about COLMAP depth to make Ground Truth depth map for Removal NeRF Dataset provided by SpinNeRF. We conducted a comprehensive evaluation of the dataset using several monocular depth estimation techniques. The detailed depth metrics could be found in Table 2. Given the extensive variation in depth distances encompassed by our evaluation dataset, we choose  $\delta_1$  depth metric to assess the adaptability and robustness of different methods across diverse depth scales as it captures variations in performance that might be obscured by more conventional depth metrics. Our finding is **ZoeDepth is the best method to obtain depth map in removal NeRF dataset**, the predicted depth values have an overlap of more than 94% with the true values, far more than EcoDepth and DepthAnything. The depth map results could be found in Figure 2, we can also see from the depth map results that ZoeDepth could describe more image details, such as object shape and edge information.

Table 2: Different Monocular Depth Estimation in Removal NeRF

Methods	Dataset	RMSE ↓	$\delta_1$ ↑	$\log_{10}$ ↓	Depth Density
ZoeDepth	Dataset1	0.102	0.526	0.146	0.968
	Dataset2	0.034	0.994	0.026	0.991
	Dataset3	0.026	0.997	0.024	0.991
	Dataset4	0.074	0.946	0.290	0.887
	Dataset5	0.035	0.984	0.016	0.981
	Dataset6	0.045	0.999	0.020	0.987
	Dataset7	0.032	0.993	0.021	0.983
	Dataset8	0.064	0.989	0.028	0.849
	Dataset9	0.035	0.989	0.017	0.911
	Dataset10	0.063	0.989	0.023	0.811
Depth Anything	Dataset1	0.173	0.058	0.636	0.968
	Dataset2	0.305	0.257	0.213	0.991
	Dataset3	0.287	0.225	0.207	0.991
	Dataset4	0.264	0.325	0.196	0.887
	Dataset5	0.449	0.363	0.189	0.981
	Dataset6	0.325	0.274	0.159	0.987
	Dataset7	0.325	0.247	0.250	0.983
	Dataset8	0.638	0.154	0.341	0.849
	Dataset9	0.356	0.218	0.222	0.911
	Dataset10	0.496	0.261	0.216	0.811
ECoDepth	Dataset1	0.075	0.496	0.130	0.968
	Dataset2	0.054	0.953	0.045	0.991
	Dataset3	0.032	0.994	0.022	0.991
	Dataset4	0.093	0.824	0.058	0.887
	Dataset5	0.065	0.962	0.037	0.981
	Dataset6	0.073	0.920	0.032	0.987
	Dataset7	0.106	0.621	0.084	0.983
	Dataset8	0.122	0.893	0.048	0.849
	Dataset9	0.062	0.939	0.036	0.911
	Dataset10	0.168	0.625	0.083	0.811

**Different Depth Priors Comparison in Removal NeRF** In order to further evaluate the effect of different depth estimation methods on removing objects from NeRF, we followed the previous experimental results, taking SpinNeRF as an example, and strictly evaluated the quality of the result by comparing its original method and the combined ZoeDepth monocular depth estimation method. The detailed comparison results could be found in Table 3, the complete depth of original SpinNeRF is provided by DSNeRF, we can see that PSNR of rendered results improved into 23.451, and time consumption is greatly reduced when utilizing ZoeDepth replaced complete depth. And some inpainting process results with different depth priors could be found in Figure 3, we found that ZoeDepth has better performance on the shape, position and depth of objects, whether it is depth estimation of the original image or after removing the object.

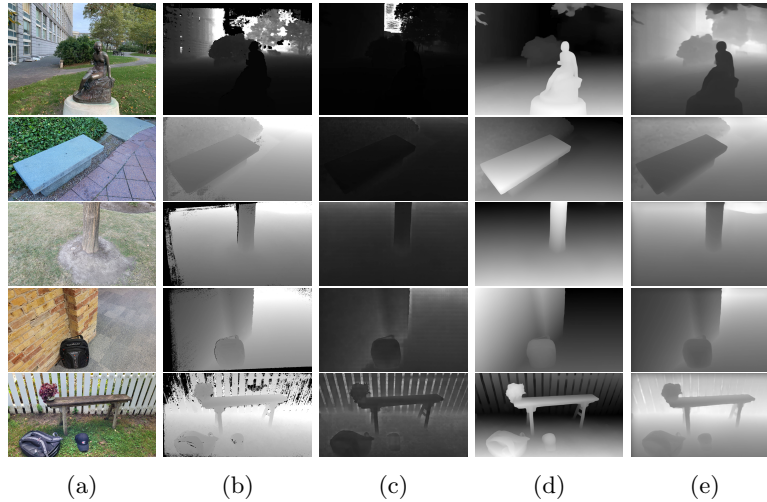


Fig. 2: Estimated Depth Map Comparison on Removal NeRF Dataset, column (a) is input image, (b) is depth map from COLMAP dense depth reconstruction, (c) is depth map from EcoDepth, (d) is depth map from Depth Anything, (e) is depth map from ZoeDepth

Table 3: The Effect of Different Depth Priors in Removal NeRF

Model	Depth Priors	PSNR $\uparrow$	SSIM $\uparrow$	Time $\downarrow$
Spin NeRF	Complete Depth	21.943	0.192	44.5s/per image
	ZoeDepth	23.451	0.192	0.58s/per image

We also visualized the training process of integrating different depth priors in SpinNeRF, details could be found in Figure 4. We found the loss value of the model gradually decreases, and the PSNR value gradually increases as the number of iterations increases. In Figure 4 (b), when ZoeDepth is integrated with SpinNeRF, at the same number of iterations, compared with the DSNeRF depth priors, the loss of SpinNeRF model is smaller and more stable, PSNR also performs better than DSNeRF depth priors. The detailed comparison of rendered qualities could be found in Figure 5, the same column represent the same rendered image sequence, and (a) (b) (c) are SpinNeRF rendered results with DSNeRF depth priors, (d) (e) (f) are SpinNeRF rendered results with ZoeDepth depth priors, rendered quality with ZoeDepth is better at the border portion of the image, such as the rendering of the wall.

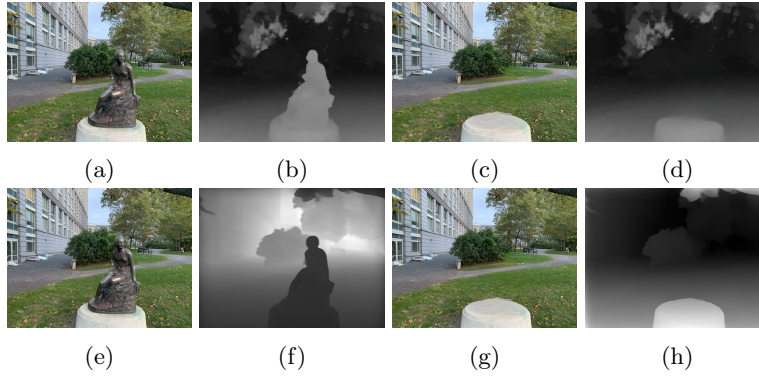


Fig. 3: Depth Map Comparison on Input Image and Inpainted Image. (a) is the input image, (b) is depth map obtained by DSNeRF priors, (c) is inpainted image, (d) is inpainted depth map, (e) is the same input image, (f) is depth map obtained by ZoeDepth, (g) is inpainted image, (h) is inpainted depth map

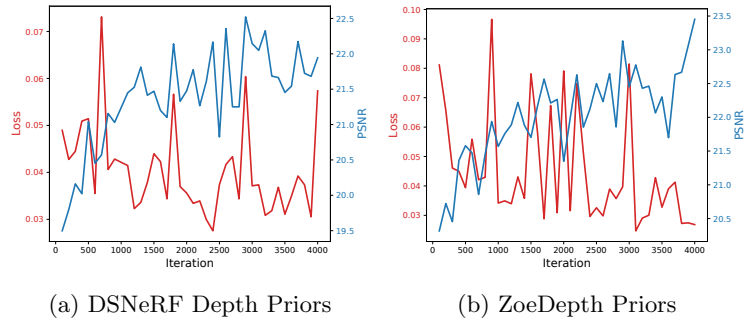


Fig. 4: SpinNeRF Training progress with Different Depth Priors

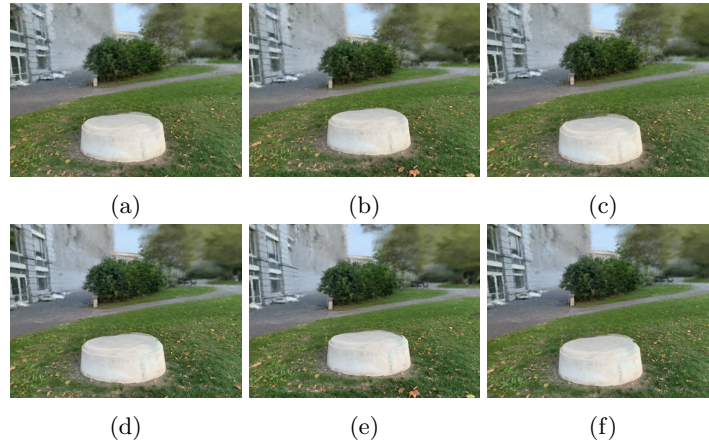


Fig. 5: Rendered Views Comparison on SpinNeRF and SpinNerf with ZoeDepth



## 5 Conclusion

This paper integrate depth priors with SpinNeRF architecture, specifically employing ZoeDepth for enhanced removal NeRF performance. Our systematic evaluation of COLMAP’s dense depth reconstruction on KITTI dataset validates its utility as a cost-effective alternative to traditional Ground Truth depth acquisition, offering a viable solution in economically restrictive scenarios. Additionally, our investigation into various monocular depth estimation methods has identified ZoeDepth as the superior technique, providing high-quality depth priors with reduced computational load. The integration of ZoeDepth with SpinNeRF not only refines object removal efficacy but also elevates the overall robustness and quality of NeRF-rendered scenes. These enhancements highlight the potential of monocular depth estimation in NeRF technology, providing options for more accurate and economically feasible 3D scene reconstruction and analysis in future human-robot digital twin systems.

## References

1. Ben Mildenhall, Pratul P Srinivasan, Matthew Tancik, Jonathan T Barron, Ravi Ramamoorthi, and Ren Ng. Nerf: Representing scenes as neural radiance fields for view synthesis. *Communications of the ACM*, 65(1):99–106, 2021.
2. Shenglin Wang, Jingqiong Zhang, Peng Wang, James Law, Radu Calinescu, and Lyudmila Mihaylova. A deep learning-enhanced digital twin framework for improving safety and reliability in human–robot collaborative manufacturing. *Robotics and computer-integrated manufacturing*, 85:102608, 2024.
3. Bangbang Yang, Yinda Zhang, Yinghao Xu, Yijin Li, Han Zhou, Hujun Bao, Guofeng Zhang, and Zhaopeng Cui. Learning object-compositional neural radiance field for editable scene rendering. In *Proceedings of the IEEE/CVF International Conference on Computer Vision*, pages 13779–13788, 2021.
4. Ashkan Mirzaei, Tristan Aumentado-Armstrong, Konstantinos G Derpanis, Jonathan Kelly, Marcus A Brubaker, Igor Gilitschenski, and Alex Levinshstein. Spin-nerf: Multiview segmentation and perceptual inpainting with neural radiance fields. In *Proceedings of the IEEE/CVF Conference on Computer Vision and Pattern Recognition*, pages 20669–20679, 2023.
5. Silvan Weder, Guillermo Garcia-Hernando, Aron Monzspart, Marc Pollefeys, Gabriel J Brostow, Michael Firman, and Sara Vicente. Removing objects from neural radiance fields. In *Proceedings of the IEEE/CVF Conference on Computer Vision and Pattern Recognition*, pages 16528–16538, 2023.
6. Kangle Deng, Andrew Liu, Jun-Yan Zhu, and Deva Ramanan. Depth-supervised nerf: Fewer views and faster training for free. In *Proceedings of the IEEE/CVF Conference on Computer Vision and Pattern Recognition*, pages 12882–12891, 2022.
7. Andreas Geiger, Philip Lenz, and Raquel Urtasun. Are we ready for autonomous driving? the kitti vision benchmark suite. In *2012 IEEE conference on computer vision and pattern recognition*, pages 3354–3361. IEEE, 2012.
8. Martin Riedmiller and A Lernen. Multi layer perceptron. *Machine Learning Lab Special Lecture, University of Freiburg*, 24, 2014.
9. Qianyi Wu, Xian Liu, Yuedong Chen, Kejie Li, Chuanxia Zheng, Jianfei Cai, and Jianmin Zheng. Object-compositional neural implicit surfaces. In *European Conference on Computer Vision*, pages 197–213. Springer, 2022.

10. Roman Suvorov, Elizaveta Logacheva, Anton Mashikhin, Anastasia Remizova, Arsenii Ashukha, Aleksei Silvestrov, Naejin Kong, Harshith Goka, Kiwoong Park, and Victor Lempitsky. Resolution-robust large mask inpainting with fourier convolutions. In *Proceedings of the IEEE/CVF winter conference on applications of computer vision*, pages 2149–2159, 2022.
11. Johannes Lutz Schönberger and Jan-Michael Frahm. Structure-from-Motion Revisited. In *Conference on Computer Vision and Pattern Recognition (CVPR)*, 2016.
12. Johannes L. Schönberger, Enliang Zheng, Jan-Michael Frahm, and Marc Pollefeys. Pixelwise view selection for unstructured multi-view stereo. In Bastian Leibe, Jiri Matas, Nicu Sebe, and Max Welling, editors, *Computer Vision – ECCV 2016*, pages 501–518, Cham, 2016. Springer International Publishing.
13. Bill Triggs, Philip F McLauchlan, Richard I Hartley, and Andrew W Fitzgibbon. Bundle adjustment—a modern synthesis. In *Vision Algorithms: Theory and Practice: International Workshop on Vision Algorithms Corfu, Greece, September 21–22, 1999 Proceedings*, pages 298–372. Springer, 2000.
14. Derek Hoiem, Alexei A Efros, and Martial Hebert. Recovering surface layout from an image. *International Journal of Computer Vision*, 75:151–172, 2007.
15. Ce Liu, Jenny Yuen, Antonio Torralba, Josef Sivic, and William T Freeman. Sift flow: Dense correspondence across different scenes. In *Computer Vision–ECCV 2008: 10th European Conference on Computer Vision, Marseille, France, October 12–18, 2008, Proceedings, Part III 10*, pages 28–42. Springer, 2008.
16. Suraj Patni, Aradhya Agarwal, and Chetan Arora. Ecodepth: Effective conditioning of diffusion models for monocular depth estimation, 2024.
17. Lihe Yang, Bingyi Kang, Zilong Huang, Xiaogang Xu, Jiashi Feng, and Hengshuang Zhao. Depth anything: Unleashing the power of large-scale unlabeled data, 2024.
18. Shariq Farooq Bhat, Reiner Birkel, Diana Wofk, Peter Wonka, and Matthias Müller. Zoedepth: Zero-shot transfer by combining relative and metric depth, 2023.
19. Shariq Farooq Bhat, Ibraheem Alhashim, and Peter Wonka. Adabins: Depth estimation using adaptive bins. In *Proceedings of the IEEE/CVF Conference on Computer Vision and Pattern Recognition (CVPR)*, pages 4009–4018, June 2021.
20. Stefano Gasperini, Nils Morbitzer, HyunJun Jung, Nassir Navab, and Federico Tombari. Robust monocular depth estimation under challenging conditions. In *Proceedings of the IEEE/CVF International Conference on Computer Vision (ICCV)*, pages 8177–8186, October 2023.
21. René Ranftl, Katrin Lasinger, David Hafner, Konrad Schindler, and Vladlen Koltun. Towards robust monocular depth estimation: Mixing datasets for zero-shot cross-dataset transfer. *IEEE transactions on pattern analysis and machine intelligence*, 44(3):1623–1637, 2020.
22. Yu Takagi and Shinji Nishimoto. High-resolution image reconstruction with latent diffusion models from human brain activity. In *Proceedings of the IEEE/CVF Conference on Computer Vision and Pattern Recognition*, pages 14453–14463, 2023.
23. Alexey Dosovitskiy, Lucas Beyer, Alexander Kolesnikov, Dirk Weissenborn, Xiaohua Zhai, Thomas Unterthiner, Mostafa Dehghani, Matthias Minderer, Georg Heigold, Sylvain Gelly, et al. An image is worth 16x16 words: Transformers for image recognition at scale. *arXiv preprint arXiv:2010.11929*, 2020.
24. Richard Zhang, Phillip Isola, Alexei A Efros, Eli Shechtman, and Oliver Wang. The unreasonable effectiveness of deep features as a perceptual metric. In *Proceedings of the IEEE conference on computer vision and pattern recognition*, pages 586–595, 2018.

25. Ashkan Mirzaei, Yash Kant, Jonathan Kelly, and Igor Gilitschenski. Laterf: Label and text driven object radiance fields. In *European Conference on Computer Vision*, pages 20–36. Springer, 2022.
26. Clement Godard, Oisin Mac Aodha, Michael Firman, and Gabriel J. Brostow. Digging into self-supervised monocular depth estimation. In *Proceedings of the IEEE/CVF International Conference on Computer Vision (ICCV)*, October 2019.
27. Zhou Wang, Alan C Bovik, Hamid R Sheikh, and Eero P Simoncelli. Image quality assessment: from error visibility to structural similarity. *IEEE transactions on image processing*, 13(4):600–612, 2004.